ROYAL SOCIETY
OF CHEMISTRY

Check for updates

The use of yttrium in medical imaging and therapy: historical background and future perspectives

Ben J. Tickner, [ID] [a] Graeme J. Stasiuk, [ID] [b] Simon B. Duckett [ID] [a] and Goran Angelovski [ID] *[c]

Yttrium is a chemically versatile rare earth element that finds use in a range of applications including lasers and superconductors. In medicine, yttrium-based materials are used in medical lasers and biomedical implants. This is extended through the array of available yttrium isotopes to enable roles for ^{90}Y complexes as radiopharmaceuticals and ^{86}Y tracers for positron emission tomography (PET) imaging. The naturally abundant isotope ^{89}Y is proving to be suitable for nuclear magnetic resonance investigations, where initial reports in the emerging field of hyperpolarised magnetic resonance imaging (MRI) are promising. In this review we explore the coordination and radiochemical properties of yttrium, and its role in drugs for radiotherapy, PET imaging agents and perspectives for applications in hyperpolarised MRI.

Key learning points

1. Versatility of yttrium coordination chemistry results in a vast number of complexes with variable physicochemical features.
2. The properties of a range of yttrium isotopes enable their use in radiochemistry.
3. Yttrium radioisotopes exploited for medical imaging and radiotherapy applications.
4. Suitability of yttrium for NMR investigations and new perspectives for yttrium-based hyperpolarized MRI.

Introduction

Since its discovery in the late 18th century, yttrium has been used as a material in lasers, superconductors, electrodes, and LEDs. The wide range of applications of yttrium-based materials has now extended into a variety of medical applications. As early as the 1960s, there were reports of using yttrium-doped lasers to remove lesions and ^{90}Y-labelled microspheres for radio-embolisation. Since then, the use of ^{90}Y-based materials for therapy has increased and they are now used clinically to treat a range of diseases including Cushing's disease, acromegaly, haemophilia and a wide range of cancers. Rapid technological advances have given additional momentum to its use in various medicinal diagnostic and therapeutic methods. Imaging techniques

especially have benefited, giving rise to the development of methodologies for the early stage detection of disease or early treatment response. Developments in the chemistry of yttrium have contributed significantly to this progress, providing valuable solutions through the preparation of contrast agents for different imaging modalities, or radiochemicals and other materials as therapeutics. Indeed, there are not many elements, especially not metal ions, which feature in the production of imaging agents or therapeutics as extensively as yttrium. Owing to the existence of various isotopes, yttrium and its complexes have found use in a wide range of diagnostics and therapy applications in different medical methodologies. The versatility of yttrium isotopes, which include ^{86}Y and ^{90}Y, has allowed for PET and radiotherapy, respectively, underpinned by significant research efforts and consequent reports over the past three decades. Very recently, ^{89}Y and its complexes have received noteworthy attention in an emerging field of HP-MRI, a methodology which has now been proven able to track real-time metabolism *in vivo*. In turn, yttrium has shown to be an excellent platform for the preparation of diverse agents that can be used for multiple medical purposes. In this review, we aim to provide a

[a] Centre for Hyperpolarisation in Magnetic Resonance, Department of Chemistry, University of York, Heslington, UK

[b] Department of Imaging Chemistry and Biology, School of Biomedical Engineering and Imaging, King's College London, London, UK

[c] MR Neuroimaging Agents, Max Planck Institute for Biological Cybernetics, Tuebingen, Germany. E-mail: goran.angelovski@tuebingen.mpg.de

This journal is © The Royal Society of Chemistry 2020

Chem. Soc. Rev., 2020, 49, 6169–6185 | **6169**

brief historical overview of the role of yttrium in therapy and medical imaging applications, anticipating possible advances in the years to come.

Coordination properties of yttrium

The element yttrium has atomic number 39 and is grouped as a transition metal in the periodic table, with electronic configuration $Kr4d^1 5s^2$. It exists naturally as the ^{89}Y isotope in 100% abundance, and has a nuclear spin quantum number I of 1/2 which means it can produce very narrow peaks in corresponding ^{89}Y NMR spectra.

Yttrium has often been regarded as a rare earth element because it bears little chemical similarity to its counterparts in the d-block. Namely, while it can form metal carbon bonds (various organoyttrium species have been reported),[1] its chemistry is most similar to that of the lanthanide elements. The main reason for this behaviour is the phenomenon called the lanthanide contraction, a result of poor shielding of nuclear charge by 4f electrons throughout elements in the lanthanide series (their general electronic configuration is $Xe4f^n 5d^m 6s^2$, where n = 1–14 and m = 0–1).[2] Consequently, both yttrium and the lanthanides do not exhibit the common properties of the transition metals; in fact, by strongly resembling the chemical properties of the lanthanides, yttrium itself is often regarded as a member of this series.

Some of the properties valid for yttrium and other members of this series are:

• Their overall level of reactivity is greater than that of transition metals, being instead more similar to the group 2 elements.
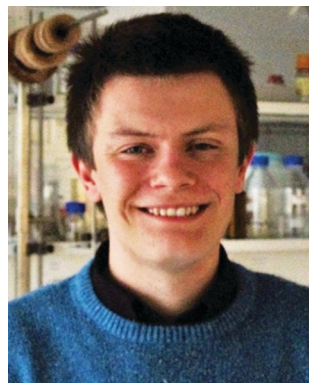
Ben J. Tickner

Ben. J. Tickner received his MChem degree from the University of York, UK in 2017. He spent time working in the group of Priv.-Doz. Dr Goran Angelovksi at the Max Planck Institute for Biological Cybernetics, Germany before starting his PhD studies with Prof. Simon Duckett at the Center for Hyperpolarisation in Magnetic Resonance at the University of York in 2017. His current research is focused on using para-hydrogen to non hydrogenatively hyperpolarize target molecules for applications in biomedical imaging, chemosensing and reaction monitoring.
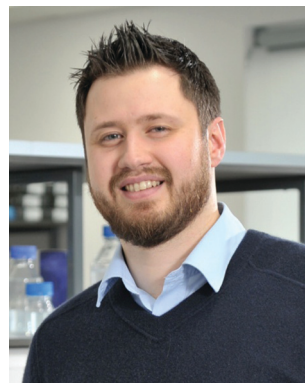
Graeme J. Stasiuk

Graeme J. Stasiuk received his MChem (2006) and PhD (2010) degrees from the University of Leicester, UK. Following a year at the French Alternative Energies and Atomic Energy Commission (CEA) in Grenoble, he joined Prof. Nick Long's group at Imperial College, London in 2011 as a PDRA. In 2014 he was appointed as a Lecturer in Molecular Imaging at the University of Hull. In 2020 he moved his research group to the Department of Imaging Chemistry and Biology at King's College London. His research focuses on the design, synthesis and validation of molecular imaging agents for all modalities.

Simon B. Duckett

Simon B. Duckett received his PhD from the University of York, UK in 1990 and afterwards undertook postdoctoral work with Prof. W. D. Jones and Prof. R. Eisenberg at the University of Rochester, USA. He returned to the University of York in 1993 and was promoted to Professor of Chemistry in 2005. Since 2010 he has been the Director of the Centre for Hyperpolarization in Magnetic Resonance at the University of York. His group studies and develops hyperpolarization techniques using para-hydrogen with a view to translation into the clinic and he has authored over 100 publications on such topics.

Goran Angelovski

Goran Angelovski holds a diploma degree in chemistry from the University of Belgrade, Serbia (2000) and PhD degree in chemistry from the University of Dortmund, Germany (2004). Since 2005, he has been a researcher at the MPI for Biological Cybernetics. In 2012, he obtained venia legendi (Habilitation) from the Faculty of Natural Sciences, University of Tübingen. Dr Angelovski is currently in the process of moving to the newly established Center for Excellence in Brain Science and Intelligence Technology (CEBSIT) of the Chinese Academy of Sciences (CAS) in Shanghai, to lead the Laboratory of Molecular and Cellular Neuroimaging and continue his research on the development of bioresponsive MRI contrast agents.

6170 | Chem. Soc. Rev., 2020, 49, 6169–6185

This journal is © The Royal Society of Chemistry 2020

• They exhibit a wide range of coordination numbers.

• They form labile ionic complexes, which are prone to the facile exchange of ligands.

• Their hydroxides are insoluble at neutral pH.

• Their coordination properties are determined by the steric factors of ligands rather than crystal-field effects.

• They prefer oxidation state +3.

• They have a preference for anionic ligands with donor atoms of rather high electronegativity.

The oxidation state +3 is the most common for yttrium, although oxidation states of 0, +1 and +2 have been reported.[3,4] Due to the above mentioned chemical properties, yttrium can exist in a number of complexes in which the central Y^{3+} ion can assume an array of different CN of up to 9 within the inner sphere. In this review, we will not cover all of the different types of complexes that can be made with yttrium, as this topic has been well explored in previous reviews and book chapters.[2,5,6] Here, we will briefly mention its complexes with the most commonly used classes of multidentate ligands as the resulting products exhibit high stability, which makes them suitable for medical applications.

Common ligands used for coordination to yttrium

Yttrium and its analogous lanthanide ions exhibit toxicity *in vivo*.[7] For this reason, it is important to ensure that complexes exhibit high thermodynamic stability, as well as being kinetically inert. This behaviour can be achieved by using multidentate ligands (Fig. 1), usually polyaminocarboxylic acids such as EDTA, DTPA, DO3A and DOTA (all abbreviations used are defined in the notes and references section at the end of the manuscript). It is important to consider ligand denticity and the chelate formation/ dissociation kinetics when anticipating applications for these chelated systems. For instance, all of these ligands rapidly form complexes, which is particularly important for the production of radiopharmaceuticals. However, hexadentate EDTA complexes have neither sufficient thermodynamic stability nor the inertness

Table 1 Thermodynamic stability constants of Y^{3+} complexes with EDTA, DTPA, DO3A and DOTA. Values for analogous Gd^{3+} complexes are provided for better comparison of properties[a]

Ligand	$\log K$ Y^{3+} complex	$\log K$ Gd^{3+} complex
EDTA	18.5	17.7
DTPA	22.5	22.2
DO3A	21.1	21.0
DOTA	24.3	25.3

[a] $\log K$ is the logarithm of the formation constant. Values taken from ref. 9.

required for medical utilisation. On the other hand, both octadentate DTPA and DOTA complexes exhibit high thermodynamic stability and their derivatives are widely used for the production of radiopharmaceuticals (see below).[8,9] Still, one should note that macrocyclic complexes based on the DOTA ligand have considerably higher thermodynamic stability than those based on the acyclic DTPA (Table 1). Namely, $\log K$ values for Y-EDTA and Y-DTPA are found to increase from 18.5 to 22.5 due to a change in denticity of the chelating ligand from 6 to 8. $\log K$ increases further to 24.3 when DOTA, an octadentate macrocyclic ligand, is employed. However, the stability is lower if the complex with the heptadentate macrocyclic ligand DO3A is formed ($\log K = 21.1$).

Similarly, the kinetic stability of the complexes formed with macrocyclic ligands is significantly higher than those of their acyclic counterparts. In a recent study, the acid-assisted dissociation of Y-DOTA and Gd-DOTA complexes was followed in 2 M and 4 M HCl by HILIC and ICP-MS.[10] The obtained half-life was 639 min and 312 min in 2 M HCl for the Y-DOTA or Gd-DOTA complexes respectively, while these values dropped to 230 min and 88 min respectively in 4 M HCl. These values are commensurate with high stability in harsh conditions. In parallel, the studied acyclic complexes show a lack of stability at less acidic conditions compared to the macrocyclic complexes. Specifically, at pH 6 and in the presence of an excess of competing cation (Zn^{2+}), these complexes undergo dissociation, resulting in half-lives of 47 min and 96 min in the presence of 5 mM Zn^{2+} for Y-DTPA and Gd-DTPA respectively, which reduced to 20 min and 52 min in the presence of 10 mM Zn^{2+}.
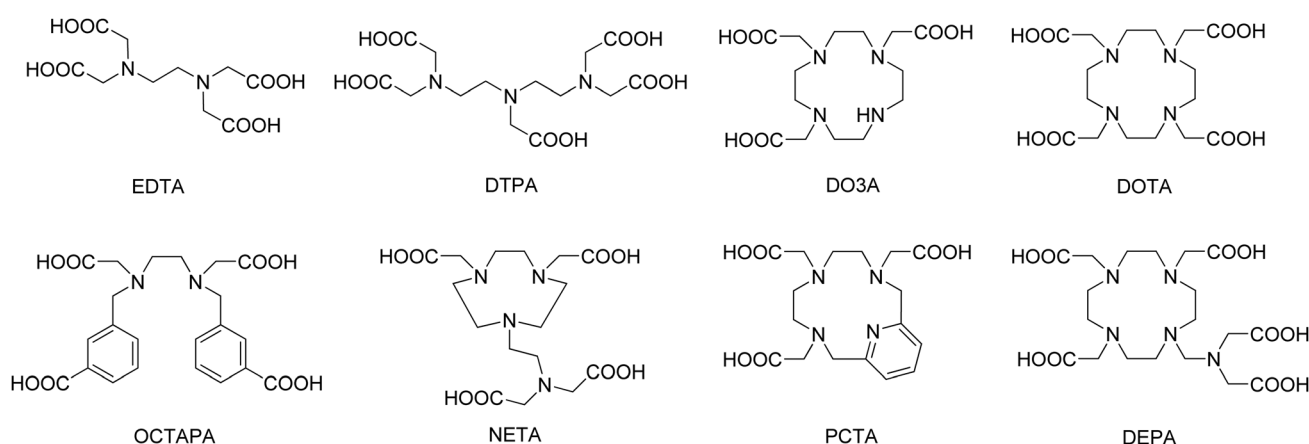

Fig. 1 Common ligands reported for chelation to yttrium that are discussed in this work.

This journal is © The Royal Society of Chemistry 2020

Chem. Soc. Rev., 2020, **49**, 6169–6185 | **6171**

The stability of these metal ion complexes can be increased by synthesising analogues with greater backbone rigidity.[11] For example, CHX-A''-DTPA is a common derivative of DTPA that contains a rigid cyclohexane group in the DTPA backbone resulting in an increase in $\log K$ from 22.5 to 24.7 for Y-DTPA and Y-CHX-A''-DTPA respectively.[12]

The geometry of the Y^{3+} complex is also affected by CN and ligand denticity. Complexes based on octadentate DOTA or DTPA typically adopt CN of 9 with an inner sphere water molecule providing an additional donor site. These coordination geometries can span distorted dodecahedron, TTP and SAP/TSAP for Y-EDTA, Y-DTPA and Y-DOTA complexes, respectively.[2,9]

TTP geometries contain ligand donor atoms arranged in triangles in three different planes, whereas SAP and TSAP isomers contain donor sites oriented in rectangles in two different planes with an additional ligand (usually water) occupying a 'capped' position (Fig. 2a). SAP and TSAP geometries are distinguished based on the angle between the two planes of donor ligands, which is typically smaller in TSAP structures. Information on these geometries comes most readily from X-ray crystal structures (Fig. 2b).[9,13,14] Moreover, the presence of nitrogen donor atoms, and the different binding conformations exhibited by these polyaminocarboxylate ligands results in formation of multiple product isomers which can often interconvert at room temperature.[8] For DTPA
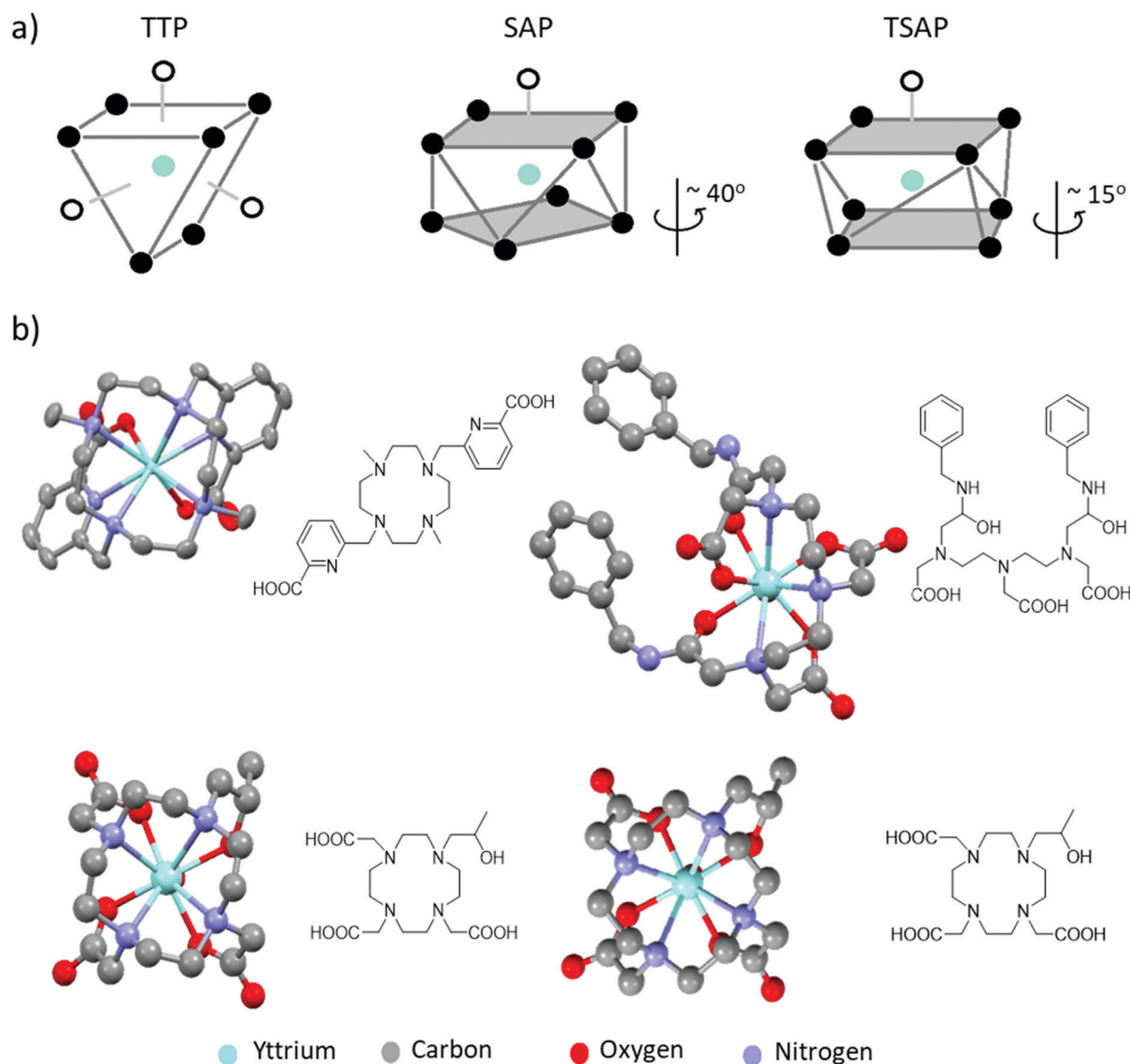

Fig. 2 (a) Representative TTP, SAP and TSAP geometries. In SAP geometries the angle of rotation between the two planes is larger than that in TSAP isomers (b) X-ray crystal structures of a range of yttrium complexes: examples of a yttrium cyclen derived complex with CN = 8 (upper left),[13] Y-DTPA-derived complex with CN = 9 adopting a TTP structure (upper right)[14] and a Y-DOTA derivative existing in both TSAP (lower left) and SAP (lower right) geometries in the same unit cell.[9] The coordinated water molecule in the latter three examples is partially obscured by the central yttrium atom. Note that all solvent of crystallisation, counterions and non-hydrogen atoms have been removed for visual clarity. Thermal ellipsoids are shown with 50% probability for those examples with atomic displacement parameters available from the crystallographic database. Otherwise, structures are shown as a ball and stick model.

6172 | Chem. Soc. Rev., 2020, 49, 6169–6185

This journal is © The Royal Society of Chemistry 2020

complexes, eight such isomers exist with the TTP geometry, which can interconvert through nitrogen inversion.[15] On the other hand, macrocycle formation reduces the degrees of freedom exhibited in DOTA complexes, thus resulting in four possible isomers that assume the above mentioned SAP and TSAP structures. The latter present more restricted coordination environments, which often result in longer distances between the metal ion and any coordinated water molecules.[9] Consequently, isomers existing in a TSAP geometry exhibit faster water exchange rates.[8] In other words, the size and steric congestion of the central metal ion and groups attached to the DOTA ligand influence the isomers formed, which affects both the NMR and MRI properties of the desired complexes. These multiple species often display quite complex spectra in corresponding ^{1}H NMR measurements provided isomer exchange is slow on the NMR timescale. However, low temperature NMR studies have been used to slow dynamic behaviour and investigate such isomers in solution.[15]

The ability of DOTA and CHX-A''-DTPA to form stable complexes with yttrium has led to their widespread use in radiopharmaceutical applications. In fact, of all the reported examples of yttrium containing radio drugs or imaging agents (see below), the significant majority are based on DOTA or CHX-A''-DTPA. Despite this, many researchers are developing new ligands that form stable yttrium complexes with fast radiolabelling conditions. These are typically based on PCTA, DEPA, OCTAPA or NETA ligands (Fig. 1).[12] A number of derivatives, variations, and combinations of these common ligand scaffolds are possible, although a full account of all ligands reported for coordination to yttrium is beyond the scope of this manuscript and has been addressed previously.[2,5,6,16] The stability or inertness of these complexes is typically determined by reference to a range of measures including thermodynamic ($\log K$)[9] and kinetic (k)[17] complex formation constants, dissociation half-lives (ι)[10] or pM values,[16] which have been described for these and related ligands elsewhere. Beside optimising their stability to match the desired metal ion, these molecules are further developed to serve as so-called bifunctional chelators. Such systems concurrently chelate the metal, while also possessing functional groups that allow further functionalization to e.g. targeting vectors, resulting in a target specific tracer or therapeutic drug (see below).[16]

Considering the similarities in coordination chemistry between lanthanides and yttrium, the general properties of these ions listed previously should be noted for different potential medical imaging and therapy applications of yttrium. Principally, selecting the ligands with sufficient thermodynamic stability, fast complex formation kinetics and good inertness is sufficient if anticipating the use of yttrium complexes for preparation of radiopharmaceuticals. Nevertheless, the coordination chemistry of the Y^{3+} complex must also be considered if the purpose is MRI application. Namely, it is well known that highly paramagnetic Gd^{3+} is routinely used as a MRI contrast agent in its chelated forms with DTPA-, DO3A- or DOTA-type ligands.[8] Due to similar ionic radii (90.0 pm and 93.8 pm for Y^{3+} and Gd^{3+} respectively), many studies have replaced gadolinium by yttrium and investigated the coordination properties of the resulting complexes by means of ^{1}H NMR.[17] However, the most recent applications of yttrium complexes in ^{89}Y NMR combined with hyperpolarisation (see below) mean a more detailed consideration of its coordination properties is warranted.

Radiochemical properties and production of yttrium isotopes

Yttrium is found in many rare earth minerals rather than as the free element and is much more common in the earth's crust than many of the transition metals such as gold and silver. It was first isolated in its elemental form in 1828 and is now commonly obtained from its ores by dissolution in sulphuric acid and fractionation of the different metal ions by ion exchange chromatography. Subsequent addition of oxalic acid allows for the isolation of yttrium oxalate precipitates. From this, oxidation can yield yttrium oxide while further reaction with hydrogen halides yield yttrium halide salts.[2] In 2014, around 7000 tonnes of yttrium oxide were produced each year, most of this by China. Yttrium is found in one naturally occurring isotope: ^{89}Y, although other isotopes including ^{90}Y and ^{91}Y are found as waste products from uranium fission. While ^{89}Y is found in many rare-earth minerals and can be found in trace amounts in living systems, it has no known role in biological processes. Studies on the toxicology of ^{89}YCl$_3$ in rats showed an increase in blood calcium concentration upon yttrium addition suggesting the replacement of calcium in bone by yttrium.[7] Calcium deposits in the liver and spleen suggest these organs are the primary targets of intravenously injected yttrium.

Currently, no fewer than 34 radionuclides of yttrium, from ^{76}Y to ^{109}Y, have been synthesized and observed.[18] While ^{86}Y, ^{87}Y, ^{88}Y, ^{90}Y and ^{91}Y have half-lives of 14.7 hours, 79.8 hours, 106.6 days, 64.1 hours, and 58.5 days respectively, all other yttrium isotopes (excluding the naturally abundant ^{89}Y) are much shorter lived with half-lives of less than a few hours. The main isotopes of yttrium can be grouped into two types depending on their main decay processes (β^- or β^+) and their half-lives (Table 2).

The neutron rich isotopes (^{90}Y and above) decay predominantly via β^- decay (electron emission) in which a neutron is converted into a proton releasing an electron and an antineutrino to form zirconium species. The kinetic energy released from rapid deceleration of these high energy electrons through interaction with surrounding matter produces radiation, which can be converted into photons. Alternatively, decay of those proton rich isotopes (^{88}Y and below) can occur via β^+ decay (positron emission), in which protons convert into neutrons releasing a positron and a neutrino to form strontium species. Those radioisotopes that exhibit β^+ decay can be used for PET imaging, which typically includes isotopes such as ^{11}C, ^{13}N, ^{15}O, ^{18}F, ^{68}Ga or ^{89}Zr.

This journal is © The Royal Society of Chemistry 2020

Chem. Soc. Rev., 2020, 49, 6169–6185 | 6173

Table 2 Half-lives and main decay processes for the most common yttrium isotopes. Those radionuclides ranging from [76]Y to [84]Y and [94]Y to [109]Y are omitted due to half-lives shorter than a few minutes

Isotope	Abundance	Half live	Main decay process	Main decay product	Applications	Ref.
[85]Y	Synthetic	2.7 hours	β^+	[85]Sr	N/A	18
[86]Y	Synthetic	14.7 hours	β^+	[86]Sr	PET	18 and 20
[87]Y	Synthetic	3.4 days	β^+	[87]Sr	PET	18 and 20
[88]Y	Synthetic	106.6 days	β^+	[88]Sr	PET	18 and 20
[89]Y	Natural	Stable	N/A	N/A	Lasers, HP-MRI	18
[90]Y	Synthetic	2.7 days	β^-	[90]Zr	Radiotherapeutics	18 and 19
[91]Y	Synthetic	58.5 days	β^-	[91]Zr	N/A	18
[92]Y	Synthetic	3.5 hours	β^-	[92]Zr	N/A	18
[93]Y	Synthetic	10.2 hours	β^-	[93]Zr	N/A	18

[90]Y is a good candidate for radiotherapy as it releases high energy β^- particles that have strong penetration of the surrounding tissues (11 mm).[12] These particles can affect cell viability by causing direct damage to the structure of DNA, or they can cause indirect cell death by increasing the concentration of toxic free radicals present in cells.[6] The conjugation of such radioisotopes to antibodies or other cancer directing groups help restrict secondary damage and focus the benefits to areas of cancer; this forms the basis of radiopharmaceuticals which are discussed later.

Many radioactive yttrium isotopes have important medical uses with [86]Y being used for PET imaging and ^{90}Y for radiotherapeutics. The synthesis, separation, and isolation of these isotopes is clearly very important. A summary of the first report of each synthetic yttrium isotope, and its initial synthesis, is given by Nystrom *et al.*[18] Briefly, ^{90}Y isotopes were first made in 1937 from high energy neutron bombardment of [89]Y, although separation of ^{90}Y from [89]Y is extremely challenging. For *in vivo* applications, ^{90}Y is now more commonly made from ^{90}Sr, one of the waste products from the fission of [235]U (Scheme 1).[6,19]

For medical applications, it is important that ^{90}Y can be synthesised free from its parent ^{90}Sr isotope. [90]Sr displays similar behaviour to calcium and is also known to be deposited in bone causing a range of health concerns including leukaemia and bone cancers. Separation of this toxic precursor is therefore essential for any use of ^{90}Y as an *in vivo* probe. Methods were developed to separate these two ions as early as the 1950s, using ion exchange principles to exploit the different charges and preferred oxidation states of strontium and yttrium salts.[19]
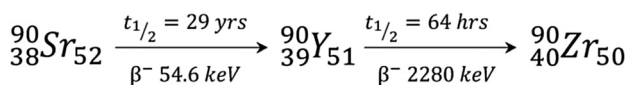
Lighter radioactive isotopes of yttrium including [86]Y and [88]Y are often produced by neutron bombardment of [89]Y.[18,20] There are three main precursors used for the synthesis of isotopes such as [86]Y, which include enriched [86]Sr, [88]Sr, and natural Rb (Scheme 2). Bombardment of Rb with alpha particles to form [86]Y and the (p,3n) reaction in which [88]Sr nuclei absorb a proton and release 3 neutrons are not commonly used due to the
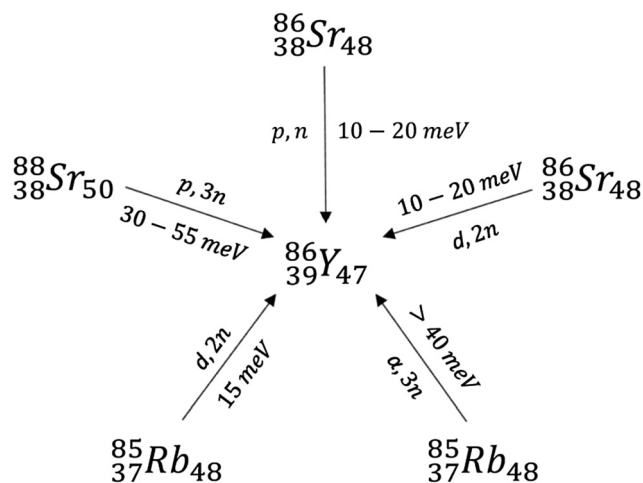
Scheme 2 Routes that lead to the formation of [86]Y isotopes.

high 30–55 keV energies of the alpha particle (α) or protons necessary. These energies are higher than those that can be produced in small synchrotrons.[20] Commonly, the (p,n) reaction from an enriched [86]Sr precursor is used due to the high purity of the resulting [86]Y.[20] Bombardment of a typical [86]SrCO$_3$ target in the presence of HCl, NH$_4$OH, H$_2$O, and La^{3+} yields mixtures containing [86]Y(OH)$_3$, which are typically separated using centrifugation and ion exchange chromatography. Subsequent addition of α-hydroxybutyrate and heating yields carrier-free [86]Y.[20] Alternatively, separation of Sr(OH)$_3$ and Y(OH)$_3$ can occur *via* electrochemical methods.[20]

Similar isotopes including [88]Y can also be produced by irradiation of a SrCl$_2$ target and subsequent separation using a cation exchange resin. These separation techniques are highly effective and can give batch yields of 3.5 GBq and 35 MBq for [86]Y and [88]Y respectively with low impurities (<3% [87]Y and <0.01 ppm Sr).[20] The production of many different yttrium isotopes using cyclotron-based approaches, and their separation is an active area of research.

Yttrium-containing materials for medical purposes

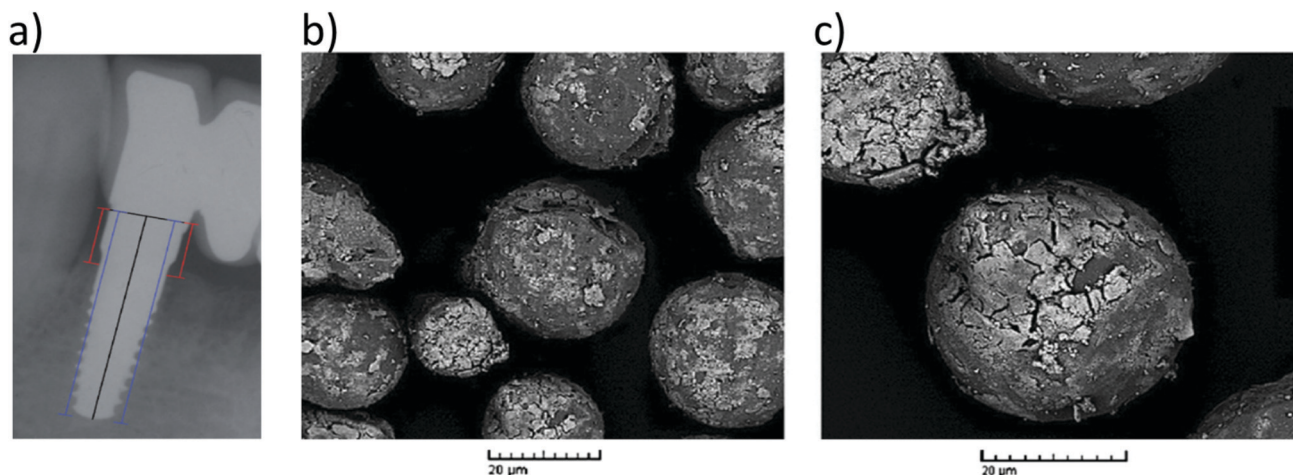Yttrium has a wide range of medical uses including as radiopharmaceuticals, lasers, and implant coatings. A range of

Scheme 1 Radiochemical reaction showing ^{90}Y formation from its parent ^{90}Sr isotope and its decay into stable [90]Zr.

Fig. 3 The use of yttrium in materials for medical purposes. (a) Radiographic control of a yttrium stabilised zirconia dental implant 24 months after surgery. Reproduced with permission from ref. 22. Copyright © 2012, Medicina Oral S. L. (b) and (c) Examples of typical scanning electron microscope (SEM) images of yttrium-containing microspheres. Reproduced with permission from ref. 25. Copyright © 2014, Springer Nature.

yttrium containing materials including yttrium fluoride nanoparticles have antibacterial properties and can be used to reduce bacterial colonisation of implanted surfaces.[21] The use of yttrium stabilised zirconia as materials for dental implants has also been reported (Fig. 3a).[22] Here, yttrium finds use in stabilising cubic polymorphs of zirconia which are usually unstable because of the large changes in volume that result upon moving between different polymorphs. This is prevented by substitution of Y^{3+} into the crystal lattice of the smaller Zr^{4+} ion to produce doped zirconia that is stable over a wider temperature range.[22]

The addition of yttrium to enhance material properties is also observed in the operation of neodymium doped yttrium aluminium garnets (Nd:YAG), which were first demonstrated in 1964 and have since been used to treat a wide range of medical ailments.[23] Nd:YAG lasers emitting light at 1064 nm are most commonly used for thermotherapy, in which lesions can be removed from a surface through laser ablation.[23] Lasers of this type can cut tissue with high precision, without causing thermal damage to the surrounding areas due to the absorption of laser light by water in nearby tissues. In the 1980s, bladder, penile, and oesophageal tumours were treated with endoscopic laser therapy and the range of cancers treated using this approach has increased since then.[23] Such lasers are also used in minor cosmetic procedures ranging from laser hair removal and wart removal to liposuction.

Other yttrium based therapies have been developed that rely not on the addition of naturally occurring [89]Y to enhance the properties of materials such as lasers or ceramic coatings, but rather to exploit the radiochemical properties of radioactive ^{90}Y in materials or complexes. Some of the earliest uses of ^{90}Y agents include its incorporation into microspheres for radioembolisation, which has been used clinically since the 1960s. Radioembolisation is a non-invasive method used to treat cancers or internal bleeding, in which a radionuclide in a microsphere is used both to block blood delivery to a site of cancer, and to deliver the β^- radiation necessary to promote cancer cell death. This is commonly used to treat unresectable cancers (which cannot be completely removed by surgery), in organs such as the liver and involves injection of the microspheres into the hepatic artery.[24] Currently, microspheres are made from either glass[24] or resin (Fig. 3b and c).[22,25] The diameter and therefore the properties and radioactive doses of these microspheres can be altered to achieve the desired properties. Commonly, these microspheres are synthesised via sol–gel chemistry or spraying techniques to achieve beads containing yttrium oxides of a desired diameter.[25] Subsequent neutron bombardment yields the radionuclide [90]Y.

[90]Y can be incorporated into a range of other materials including needles and rods. [90]Y rods have been implanted into the pituitary gland in order to treat Cushing's disease.[26] This disease results from heightened levels of the hormone cortisol caused usually by steroid overuse or adrenal or pituitary tumours. Implantation of ^{90}Y can have therapeutic effects on such pituitary tumours[26] and reduce the effects of acromegaly, a hormonal condition caused by excess production of growth hormone by the pituitary gland.[27] Other ^{90}Y containing materials such as ^{90}Y needles have been used for synvectomy. This technique removes synovial tissues around joints which often become inflamed in conditions like rheumatoid arthritis. This inflamed tissue can be removed surgically or by using drugs or radiotherapeutics such as ^{90}Y to reduce the mass of inflamed tissue.[28] Injection of ^{90}Y into joints of haemophilia patients has been found to induce fibrosis and reduce internal bleeding in joints.[29] Such treatments have previously used radioactive isotopes such as [198]Au, although isotopes including ^{90}Y, [186]Re and [169]Er are preferred. Agents such as ^{90}Y silicate have a particle size of 0.1 μm which is around 50 times larger than those of the previously used colloidal [198]Au system which prevents unwanted spread of the agent to other sites via the lymphatic system.[29]

Yttrium-containing complexes for therapy

Clinically approved radioagents based on ^{90}Y have been used for the treatment of various types of cancers. These are based on the conjugation of ^{90}Y chelators such as DTPA or DOTA to cell receptor targeting motifs (peptides/antibodies) to direct the therapy to the cancer cells. For example, the conjugation of DTPA or DOTA to different peptides has been used to target the chelate ions to different sites in the body. Similarly, Gd^{3+} complexes based on DOTA and its analogues have been conjugated to peptides for use as targeted MRI contrast agents. ^{86}Y complexes have been used to image the biodistribution and uptake of the analogous Gd^{3+} or ^{90}Y complex (see below).[10] Several excellent reviews on some of these agents, and the clinical studies that have been performed, exist.[5,6] Hence, here we provide only a general overview of the different types of ^{90}Y-radiopharmeceuticals and how they work.

There are several key factors in the selection of a chelator with targeting peptide/antibody for effective therapy:
• Radiolabelling conditions for the chelator.
• Kinetic/thermodynamic stability of the complex.
• Radiation half-life compared to biological half-life.

Radiolabelling conditions for ^{90}Y complexes vary with the choice of chelator. DOTA-based chelators all use conditions between pH 4.5 to 6, with heating as high as 100 °C for 15 minutes to form stable complexes (Tables 3 and 4), with a high molecular activity (45–75 GBq µmol^{-1}). These harsh conditions are tolerated by small peptide targeting vectors, indicated by the use of DOTA in somatostatin radiotherapy (discussed below). DTPA has been shown to be labelled with ^{90}Y at room temperature at pH 5.5 between 5–30 minutes, giving molecular activities of around 781 MBq mg^{-1}. The resulting complex shows sufficient stability to be utilised *in vivo*. The key here is that the complex is formed at room temperature, so it can be used for antibody labelling, which is more sensitive to elevated temperatures. The half-life of ^{90}Y is 2.7 days (Table 2), which is consistent with the biological half-life of antibodies; therefore, DTPA is more suited for conjugation to antibodies and radiolabelling with ^{90}Y.

^{90}Y based small molecule agents utilising the coordination chemistry properties of yttrium, rather than its incorporation into bulk materials, have been developed to deliver the β$^-$ radiotherapy to a specific cell type. Cancerous cells are known

Table 3 Summary of selected ^{90}Y radiotherapeutics[a]

Name	Chelator	Bioconjugate	Target	Labelling conditions	Dose	Disease	Studies	Ref.
Microspheres	N/A	N/A	N/A	Neutron bombardment of ^{89}Y microspheres for 4 days.[22]	—	Hepatocellular carcinoma	Human	24
					100–150 000 rad	Cushing's disease		26
					—	Acromegaly		27
					185 MBq	knee arthritis		28
					185–2597 mBq (knee) 74–111 mBq (elbow)	Haemophilia		29
^{90}Y-DOTATOC	DOTA	DPhe^1-Tyr^3-octreotide	Somatostatin	0.4 M NH$_4$OAc or 0.2 M NaOAc pH 5 90 °C 25 min[30]	6–32 GBq m^{-2}	Neuroendocrine tumours	Human	30
^{90}Y-DOTATATE	DOTA	Tyr^3-Thr^8-octreotate						
^{90}Y-DOTALAN	DOTA	lanreotide						30 and 32
^{90}Y-DOTANOC	DOTA	1-NaI^3-octreotide						33
^{90}Y-DOTAOC	DOTA	Octreotide						33
^{90}Y-SMT487	DOTA	DPhe^1-Tyr^3-octreotide		—	—		Primates	35
^{90}Y-Citrate	Citrate	N/A	N/A	—	1 MBq	Prostate cancer (bone metastases)	Human	35
^{90}Y-EDTMP	EDTMP	N/A	N/A	—	1 MBq	Prostate cancer (bone metastases)	Human	35 and 48
^{90}Y-Cetuximab	DOTA	Cetuximab	EGFR	—	1 MBq	Head and neck cancers	Human	37
^{90}Y-DOTA-panitumumab	DOTA	Panitumumab		—	3.7 MBq	Head and neck cancers	Human	38
^{90}Y-CHX-A″-DTPA-trastuzumab	DTPA	Trastuzumab	HER2	0.2 M NH$_4$OAc pH 5.5 37 °C 1 hour	∼3.7 MBq	HER2 tumours/ovarian cancer	Mice	39
^{90}Y-Octapa-trastuzumab	Octapa	Trastuzumab						
^{90}Y-3p-C-NETA-trastuzumab	NETA	Trastuzumab		0.25 M NH$_4$OAc pH 5.5 RT 5 min	—	Breast cancer	Mice	12
Zevalin	Tiuxetan	Ibritumomab	CD20	50 mM NaOAc RT 5 min	<1.2 GBq	Non-Hodgkin's lymphoma	Human	36
^{90}Y-Rituximab	DOTA	Rituximab		—	14.8 MBq kg^{-1}	Nodular lymphocyte predominant Hodgkin lymphoma		40

[a] Any abbreviations used are defined in the notes and references section at the end of the manuscript.

6176 | Chem. Soc. Rev., 2020, 49, 6169–6185

This journal is © The Royal Society of Chemistry 2020

Table 4 Summary of selected ^{86}Y and ^{87}Y radiotracers used for PET imaging[a]

Name	Chelator	Bioconjugate	Target	Labeling conditions	Dose	Disease	Studies	Ref.
^{86}Y-Citrate	Citrate	N/A	N/A	—	100 MBq	Prostate cancer (bone metastases)	Human	10 and 35
^{86}Y-DTPA	DTPA	N/A	N/A	Citrate buffer pH 6 80 °C 5 min	11.8–14.7 MBq	—	Rats	10
^{86}Y-DOTA	DOTA	N/A	N/A	Citrate buffer pH 6 80 °C, 30 min	11.8–14.7 MBq	—	Rats	10
^{86}Y-EDTMP	EDTMP	N/A	N/A	—	130–295 MBq	Prostate cancer (bone metastases)	Human	35 and 48
^{86}Y-SMT487	DOTA	DPhe^1-Tyr^3-octreotide	Somatostatin	—	10–40 MBq	Neuroendocrine tumours	Primates	35
^{86}Y-DOTATOC	DOTA	DPhe^1-Tyr^3-octreotide		0.15 M NH$_4$OAC pH 4.5 100 °C 15 min	77–186 MBq	Neuroendocrine tumours	Human	35 and 44
^{86}Y-CHX-A″-DTPA-octeotide	CHX-A″-DTPA	CHX-A″	—	—	—	Neuroendocrine tumours	Mice	44
^{86}Y-DOTA-ReCCMSH(Arg11)	DOTA	ReCCMSH (Arg11)	Alpha-melanocyte stimulating hormone	—	—	Melanoma	Mice	44
^{86}Y-MP2346	DOTA	MP2346	Gastrin releasing peptide receptor	—	—	PC-3 tumours	Mice	44
^{86}Y-CHX-A″-DTPA-cetuximab	CHX-A″-DTPA	Cetuximab	HER1 receptors	0.1 M NH$_4$OAC pH 5–6 RT 30–60 min	2 GBq mg^{-1}	Mesothelioma Tumors	Mice	12
^{86}Y-CHX-A″-DTPA-panitumumab	CHX-A″-DTPA	Panitumumab	HER1 receptors	—	2 MBq m^{-2}	HER1 tumours	Mice	44
^{86}Y-1B4M-DTPA-trastuzumab	DTPA	Trastuzumab	Ovarian cancer cells	—	—	Ovarian and colorectal tumours	Mice	44
^{86}Y-CHX-A″-DTPA-antimindin/RG-1	CHX-A″-DTPA	Antimindin/RG-1	Mindin/RG-1	0.1 M NH$_4$OAC pH 5–6 RT 30–60 min	29.6–39.6 MBq mg^{-1}	LNCaP tumours	Mice	12 and 46
^{86}Y-CHX-A″-DTPA-bevacizumab	CHX-A″-DTPA	Bevacizumab	VEGF-A	0.15 M NH$_4$OAC pH 7 RT 30 min	1.8–2.0 MBq	Colorectal carcinoma	Mice	12 and 47
^{87}Y-EDTMP	EDTMP	N/A	N/A	—	2 MBq	—	Mice	49

[a] Any abbreviations used are defined in the notes and references section at the end of the manuscript.

to overexpress receptors on their cell surfaces for a wide range of different proteins. This has formed the basis of drug and peptide receptor radionuclide therapy (PRRT). One such over-expressed receptor is that for somatostatin, a growth hormone-inhibiting hormone, which inhibits the release of a range of hormones including insulin and glucagon *via* its interaction with G-coupled protein receptors.[30] Conjugation of radionu-clides to somatostatin analogues allow for incorporation of the agent into the cancerous cell, localising β$^−$ emission in the area of cancer. Somatostatin was an important synthetic target for many years and many groups used solid phase approaches to synthesise this natural product. A more potent somatostatin analogue called octreotide was first synthesised in 1979 and derivatives have since been conjugated to ^{90}Y coordinating motifs such as DTPA and DOTA derivatives. Currently, ^{90}Y-DOTATOC is the most commonly reported ^{90}Y radiotherapy that targets somatostatin receptors (Fig. 4).[30] It has commonly been used to treat tumours of the endocrine or nervous systems although other cancers such as glioma and meningioma have also been targeted.[30] Similar systems such as ^{90}Y-DOTATATE,[31] ^{90}Y-DOTALAN,[32] and ^{90}Y-DOTANOC[33] have also been reported, which involve the conjugation of ^{90}Y to other octreotide-like peptides that target somatostatin receptors. The selection of either the chelator or the final charge of the complex can alter the biodistribution of the therapeutic agent (or imaging agent,
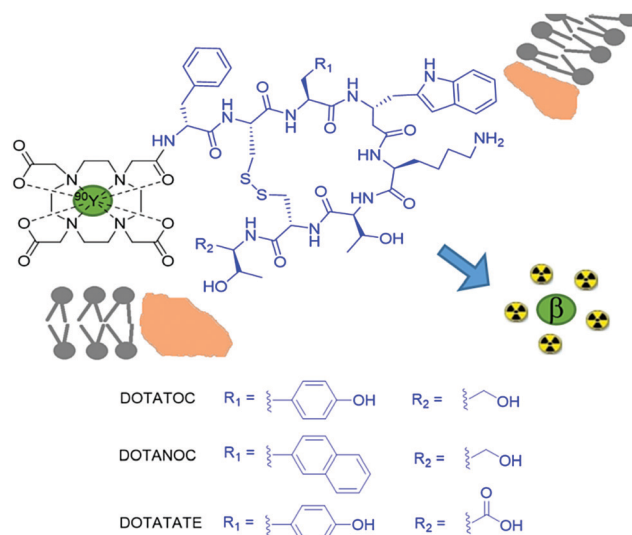

Fig. 4 ^{90}Y complexes for targeted therapy. Conjugates of ^{90}Y and its macrocyclic chelator DOTA (black) with an octreotide-like peptide (blue) can bind to over expressed somatostatin receptors on cancer cell surface membranes. Upon transport into the cancerous cell, the emitted β radiation has therapeutic effects.

see later), resulting in different levels of accumulation in target sites.

This journal is © The Royal Society of Chemistry 2020

Chem. Soc. Rev., 2020, 49, 6169–6185 | 6177

It must be stated that there has been a switch in the clinic towards ^{177}Lu in PRRT, which is due to the β^- range decreasing from 11 mm to 2 mm, thus reducing non-specific cross fire side effects.[12] This move has also brought the use of combination therapy, using both ^{90}Y-DOTATATE and ^{177}Lu-DOTATATE, which aid these dosimetry calculations, although this matched pair has advantages compared to using just ^{90}Y-DOTATATE.[31] The same is valid for the ^{90}Y-DOTATOC analogue.[34]

An accurate prediction of the radiation dose provided by exposure to these ^{90}Y agents is challenging. In the 1990s analogous ^{111}In agents were used although this isotope is now rarely deployed due to differences in the biochemical behaviours of ^{90}Y and ^{111}In that have since been observed.[12] Attempts to reduce the dose administered (3.7 GBq m^{-2}) of ^{90}Y PRRT, have resulted in the match pair isotope [86]Y being more commonly used to map where the therapy will go *in vivo via* PET (see below). This allows clinicians to monitor in each patient where the somatostatin positive tumours and the non-specific localisation of the tracers are, such that an appropriate dose of ^{90}Y can be adminstered.[35]

In recent years, many other over expressed surface receptors on cancer cells have been targeted for radiotherapy with ^{90}Y complexes. Many lymphomas express specific antigens (CD20) that are not expressed on normal cell surfaces. This provides a route for targeted radiotherapy in which radionuclides are attached to antibodies specific to cancer cells. Since the development of ^{90}Y-DOTATOC, antibody conjugates such as ^{90}Y-ibritumomab tiuxetan (Zevalin) have been developed for this purpose, consisting of a ^{90}Y coordinating group (tiuxetan) and the anti-CD20 antibody ibritumomab (Fig. 5a).[36] In addition to ^{90}Y loaded microspheres and ^{90}Y-DOTATOC, Zevalin has also received FDA approval for human use (in 2002) and has been shown to improve survival rates in patients (over a 7 year period).[36]

Over recent years many other antibody based ^{90}Y therapies have been developed involving cetuximab,[37] panitumumab,[38] trastuzumab[39] and rituximab.[40] While rituximab also targets CD20, other therapies have targeted receptors such as EGFR (cetuximab and panitumumab) or HER2 (trastuzumab) (Table 3). This is largely due to the matching half-life of [90]Y (2.7 days) and the biological half-life of antibodies.[39] Such agents are typically used to treat non-Hodgkin lymphoma, a group of blood cancers that develop from white blood cells. The conjugation of panitumumab to a ^{90}Y-DOTA or ^{90}Y-DTPA based group has been used to treat head and neck cancers in a mouse model.[38] The related cetuximab is able to cross the blood brain barrier. Upon the administration of ^{90}Y labelled cetuximab, accumulation in brain tumours was observed and studies have investigated its effect on human cancer cell lines.[37] [90]Y radiolabelling was found not to affect the action of cetuximab. Radiotherapy using ^{90}Y labelled rituximab has yielded complete metabolic remission for patients with Nodular lymphocyte-predominant Hodgkin lymphoma[40] (Fig. 5b and c) and the use of new ^{90}Y labelled antibody conjugates of this type, and others, are expected to increase in the future.
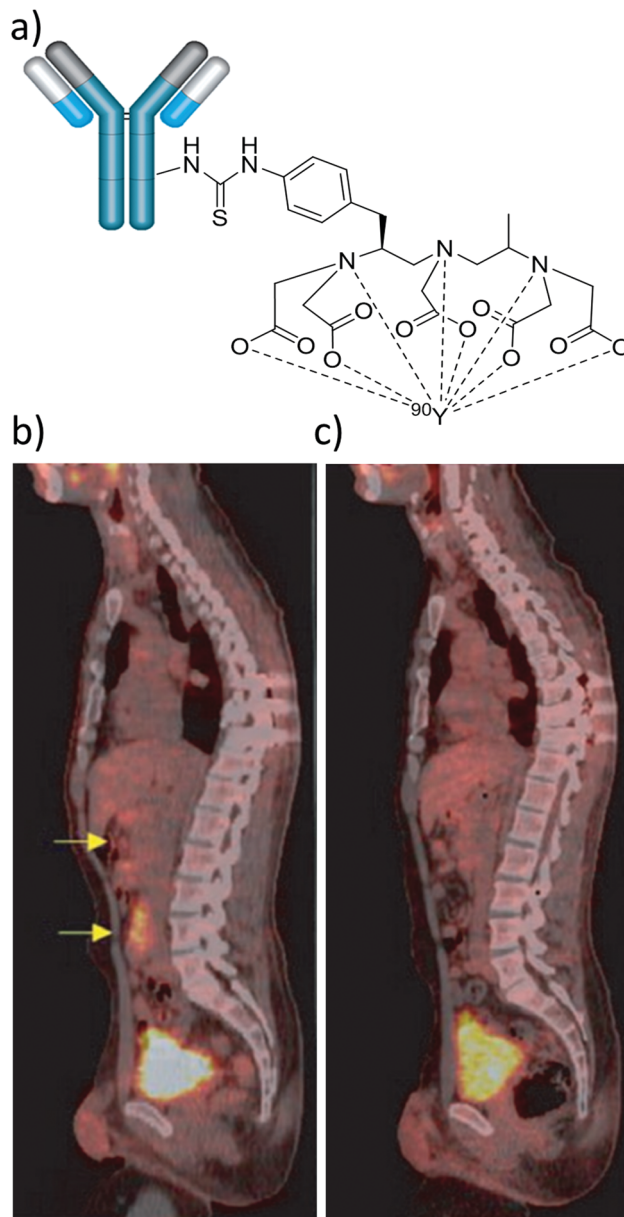

Fig. 5 Applications of ^{90}Y labelled antibody-based therapy. (a) Depiction of Zevalin, a conjugate of anti-CD20 antibody ibritumomab and the DTPA-derived ^{90}Y chelator tiuxetan. (b) and (c) Example of [18]FDG PET/CT sagittal slices showing retroperitoneal lymph nodes (yellow arrows) of a 38 year old male patient with nodular lymphocyte-predominant Hodgkin lymphoma (b) before and (c) 6 months after treatment with ^{90}Y-rituximab radioimmunotherapy. Adapted with permission from ref. 40. Copyright © 2018 John Wiley & Sons A/S.

PET imaging using yttrium-based tracers

Imaging techniques such as PET can take advantage of those radionuclides that exhibit β^+ decay. The production of high energy positrons during this decay can be detected indirectly through the production of two gamma photons formed from annihilation of positrons with surrounding electrons in tissues. This annihilation of antiparticles will occur when the high

6178 | Chem. Soc. Rev., 2020, 49, 6169–6185

This journal is © The Royal Society of Chemistry 2020

energy positrons have travelled from the source of the radio-tracer and have lost sufficient kinetic energy to interact with surrounding electrons. Encounters between positron and electron will produce two gamma photons moving in opposite directions. These are distinguished from background photons by detecting photon pairs arriving at a camera placed around the patient within short time intervals. The most common radiolabelled probe used clinically is ^{18}F-fluorodeoxyglucose ([18]FDG), which allows glucose uptake to be imaged using PET.[41]

Imaging the uptake and biodistribution of ^{90}Y agents is very important in determining the dosage and side effects of such therapies. Dual therapies in which injected agents have the therapeutic effects of ^{90}Y based agents whilst retaining the potential to be simultaneously imaged inside the body are clearly essential. Imaging ^{90}Y is a challenge and there have been many attempts to address this including imaging the Bremsstrahlung radiation emitted from the β^+ decay of [90]Y.[5] While ^{90}Y decays predominantly by β^+ processes, it has been known since the 1950s that minor decay via positron emission (34 ppm, 0.003%) is possible. In the past, the most common approach has been to administer the same ^{90}Y based agent coordinated to a different radionuclide that undergoes positron emission and can be imaged by PET. Co-administration of other radionuclides such as [44]Sc, ^{68}Ga, ^{111}In or ^{177}Lu is commonly used as a route to image the progress, uptake, dosage, or biodistribution of the analogous ^{90}Y radiotherapeutic agent at the target site or in off-site organs via PET or SPECT (isotope dependent).[31,34]

It has recently been shown that ^{90}Y distribution can be quantified using direct positron emission from [90]Y.[42] This imaging route faces challenges from low positron emission and high background signals from Bremsstrahlung radiation, although despite this it can give some route to imaging ^{90}Y distribution.[42] Direct imaging of ^{90}Y via either Bremsstrahlung radiation or β^+ decay is feasible. For instance, combined Bremsstrahlung SPECT and ^{90}Y PET/CT imaging of ^{90}Y labelled microspheres was achieved by injecting them into an area of metastatic cholangiocarcinoma in the left hepatic lobe (Fig. 6).[43]

A PET image using [18]FDG is also included for comparative purposes. Here, Bremsstrahlung SPECT imaging gives a diffuse response in the area of the tumour while ^{90}Y PET/CT gives a more localised response.[43] In this case there is poor uptake of ^{90}Y agent into the tumour and signal is much more localised in the cancerous target upon imaging with [18]FDG.

Increasingly, those yttrium isotopes such as [86]Y that do decay predominantly via β^+ emission (half-life 14.7 hours) are being investigated as potential PET imaging agents.[44] [86]Y is a non-ideal isotope for PET imaging because 67% of its β^+ decay processes are accompanied by release of gamma rays. Simultaneous γ ray emission can fall into the accepted energy window of PET scanners (350–650 keV), which results in background signals. Such background noise can lead to increased false positive detection by the PET scanner and therefore erroneous quantification of [86]Y concentration.

Methods are being developed to apply background corrections to [86]Y PET images to help alleviate these interference issues.[45] Consequently, noise in PET images of [86]Y-DOTATOC can be reduced upon background subtraction (Fig. 7).[45] In comparison, decay from the more commonly used ^{18}F isotope consists of only β decay.

Despite these challenges, the most promising use for [86]Y radiotracers is in combination with ^{90}Y radiotherapy analogues as matched pair isotopes to predict the distribution and dosimetry of subsequently injected radiotherapeutics in the same way as other PET agents (i.e. [68]Ga).[46,47] In the case of [86]Y/^{90}Y mixed pairs, the biological distribution/pharmacokinetics of the two isotopes will be identical as the chemical properties of the PET tracer and the radiotherapeutic are the same.[48] This will give clinicians the ability to predict where the treatment will go on a patient by patient basis. This means that if there is significant off site organ uptake, the optimum radioactivity dose can be given, which is expressed as maximum dose at target tissues versus tolerable dose at healthy organs. The appropriate doses of the radiotherapeutic can be given to lower the cross fire or side effects of the radiotherapy and make it more effective as a therapeutic. The standard doses of PET imaging agents administered to patients lies in the
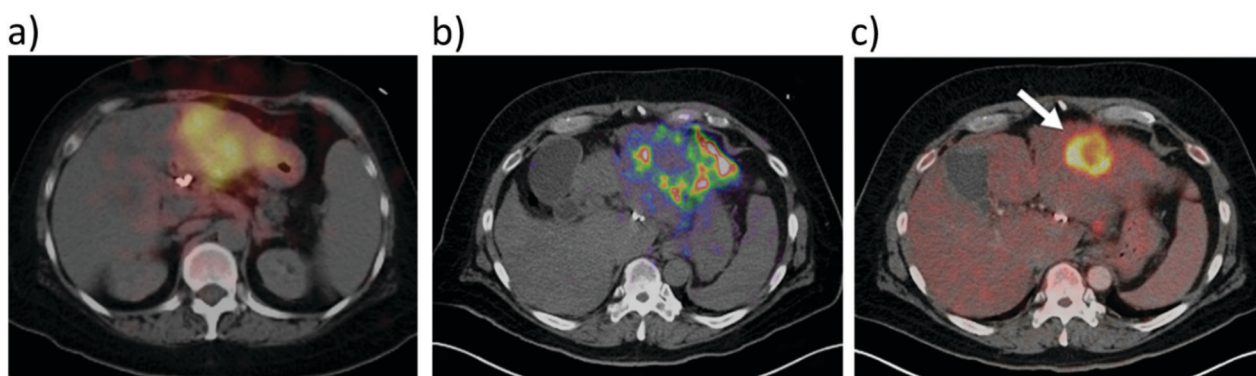

Fig. 6 Use of ^{90}Y for SPECT and PET imaging. [90]Y labelled microspheres were injected into an area of metastatic cholangiocarcinoma in the left hepatic lobe and the imaging was performed either using: (a) Bremsstrahlung SPECT, (b) ^{90}Y PET/CT, or (c) ^{18}F PET using [18]FDG prior to radioembolisation. Reproduced with permission from ref. 43. Copyright © 2014, Pasciak, Bourgeois, McKinney, Chang, Osborne, Acuff and Bradley.
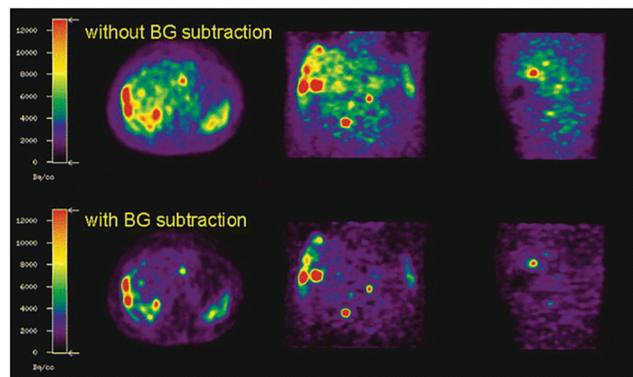
This journal is © The Royal Society of Chemistry 2020

Chem. Soc. Rev., 2020, 49, 6169–6185 | 6179

Fig. 7 Effect of background subtraction on ^{86}Y PET imaging. PET imaging of ^{86}Y-DOTATOC with and without background subtraction. Reproduced with permission from ref. 45. Copyright © 2003, Springer Nature.

1–300 MBq range, while for therapeutic isotopes it is in the 6–32 GBq m^{-2} range (Table 4). Typically, this results in a picomolar concentration range of PET tracers required to give these radiation doses. A similar approach has used PET imaging of ^{86}Y labelled analogues to predict the biodistribution and clearance pathways of analogous gadolinium based MRI contrast agents. It has been known that the use of Gd-based contrast agents can be connected with the nephrogenic system fibrosis disease, which is related to deposition of Gd^{3+} in the kidneys of patients with poor renal clearance, or can lead to deposits in the brain. In fact, it is extremely challenging to measure the biodistribution of Gd-based agents, and T_1-weighted MRI is unable to measure residual concentrations of this ion. To this end, PET imaging of ^{86}Y-DTPA has been used to track the clearance pathways of the analogous Gd-DTPA in rats (Fig. 8).[10] These images show that the injected agents are predominantly excreted through the kidneys in less than 4 hours, although a small amount of agent is retained by the kidneys and excreted over a longer time scale (images recorded up to 48 hours post injection).[10] PET images are even able to show the presence of secondary excretion pathways. For example, PET images acquired 4 hours post injection showed that the agent was present in the large intestines suggesting that hepatic clearance is also occurring (Fig. 8d).[10] The use of ^{87}Y and ^{88}Y as potential SPECT and PET tracers respectively has also been investigated.[49] In an attempt to show the broadness of different ^{90}Y- and ^{86}Y-based radiotracers for medical imaging and therapy, we have summarized their use along with the chelators, type of bioconjugates, desired targets, labelling conditions, dosages and specific applications (Tables 3 and 4).

Hyperpolarised ^{89}Y complexes as MRI probes

In contrast to PET, MRI uses magnetic field gradients and radiofrequency pulses to produce spatially and temporally resolved images of living systems. This technique involves the use of non-ionising radiation and does not require specialist facilities like those necessary for PET. Instead, it routinely
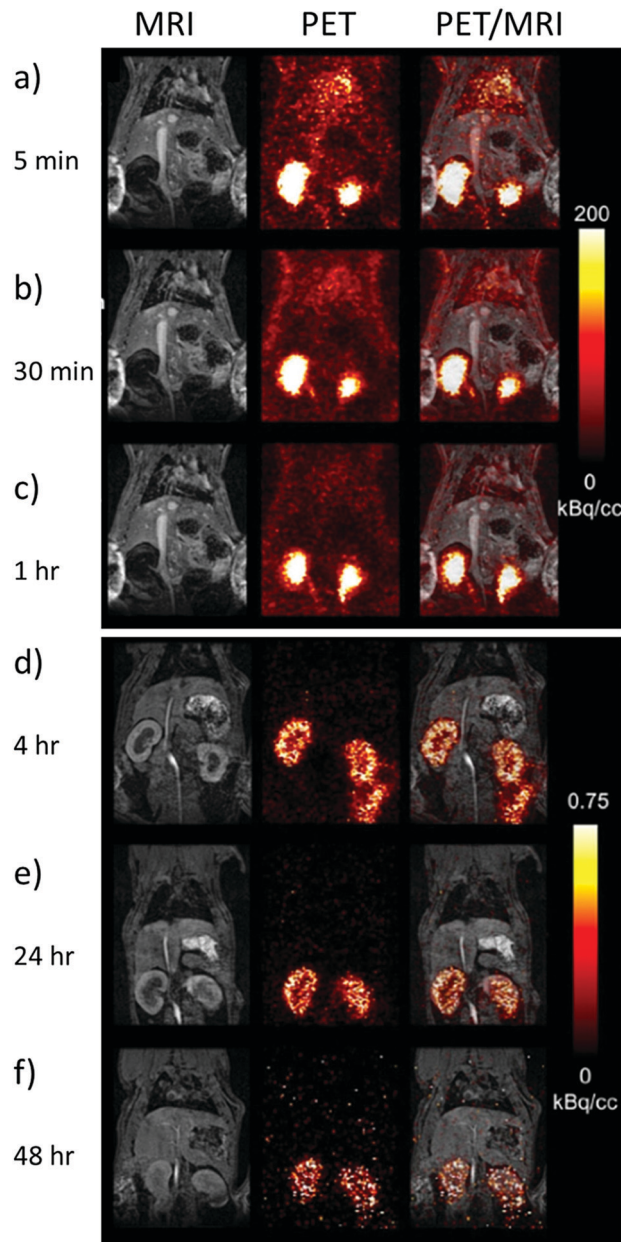

Fig. 8 PET imaging of ^{86}Y complexes as surrogates for Gd MRI contrast agents. Example MRI, PET and overlaid PET/MRI images of rats taken (a) 5 min (b) 10 min (c) 1 h (d) 4 h (e) 24 h and (f) 48 h after the injection of ^{86}Y-DTPA (11.8 MBq) and Gd-DTPA (0.6 mmol kg^{-1}). Note that the intensity scale for (a)–(c) and (d)–(f) are not the same. Reproduced with permission from ref. 10. Copyright © 2019 Wiley-VCH Verlag GmbH & Co. KGaA, Weinheim.

detects NMR-active nuclei, which in the majority of cases are water protons, where different environments are distinguished by their longitudinal (T_1) or transverse (T_2) relaxation time constants.[8] It is the low inherent sensitivity of MRI that necessitates reliance on the bulk ^{1}H$_2$O signal to convey this information. MR sensitivity is derived from small perturbations in the population of states occupying closely spaced nuclear spin energy levels in a magnetic field. While relaxation inducing agents often provide a route to improving contrast, many

6180 | Chem. Soc. Rev., 2020, **49**, 6169–6185

This journal is © The Royal Society of Chemistry 2020

researchers are turning their attention to hyperpolarisation as a non-toxic alternative to address insensitivity.[50]

Hyperpolarisation techniques such as dynamic nuclear polarisation (DNP) create non-Boltzmann population distributions across nuclear spin energy levels and can lead to MR signal gains of up to five orders of magnitude.[50] DNP can achieve this effect in heteronuclei such as ^{89}Y through transfer of polarisation from unpaired electrons. This involves microwave irradiation of a frozen glass matrix containing the ^{89}Y agent and a free radical in a magnetic field (~ 3 T) at low temperature (1–2 K). This technique of transferring the inherently greater electron polarisation to that of a proton was first suggested by Albert Overhauser in 1953 and experimentally validated by Carver and Slichter in the same year.[50] It took until 2003 for dissolution DNP (d-DNP), which involves the rapid melting of hyperpolarised solids with superheated solvent, to offer a proven route to dramatically enhance the MR signals of small molecules in solution.[50] This breakthrough has created the excitement needed to drive further development. Consequently, d-DNP has now been used in a number of clinical studies associated with the production of hyperpolarised ^{13}C tracers, of which pyruvate is the most widely reported.[50] Indeed, the *in vivo* injection and metabolic imaging of hyperpolarised ^{13}C pyruvate into humans has been used as a method to diagnose cancer.[50]

Despite the current successes of hyperpolarised ^{13}C probes, hyperpolarisation techniques can target many other heteronuclei, including ^{89}Y. ^{89}Y is an interesting nucleus for study by MR because it is non quadrupolar ($I = 1/2$) with 100% natural abundance. As living cells have no known use for ^{89}Y, there is no inherent background response and consequently its use as a medical probe provides an exciting opportunity for clinical applications. However, one should note that ^{89}Y has a gyromagnetic ratio that is around 20 times smaller than that of ^{1}H and its corresponding MR receptivity is 10 000 times smaller than ^{1}H, albeit similar to that of ^{13}C. On the other hand, early studies in the 1970s demonstrated that ^{89}Y salts exhibit long T_1 times that can exceed 100 seconds.[13] The incorporation of ^{89}Y into metal complexes was found to elongate relaxation times even further.[13] Collectively, this makes Boltzmann polarised ^{89}Y MR studies challenging as low receptivity must be overcome by signal averaging which necessitates long measurement times to overcome the long relaxation lifetime. These measurement times for thermally polarised samples can be reduced by the addition of relaxation inducing dopants, which overcome the latter effect. In contrast, long relaxation times provide the potential to detect hyperpolarised ^{89}Y nuclei *in vivo* before the hyperpolarised state decays back to its Boltzmann populated state and may provide many advantages. For example, DNP has been used to successfully hyperpolarise ^{89}Y with enhanced ^{89}Y NMR signals detected in just a single scan (Table 5).[13] Achieving this result is a substantial breakthrough as measurement of Boltzmann derived signals is challenging for the reasons given above and the DNP process is itself costly, time consuming and single shot in nature. In addition, whilst most DNP machines contain an in-built NMR spectrometer that is

Table 5 Different reported conditions for the hyperpolarization of ^{89}Y using DNP, where ε is the solution state ^{89}Y signal enhancement

Y material	Polarizing agent	Glassing matrix	Microwave frequency	Irradiation time	Microwave power	Temperature	Magnetic field	Dissolution medium	ε/fold	Ref.
YCl$_3$ (54 mM)	TEMPO (30 mM)	D$_2$O/glycerol-d_8 (10 μL, 60/40, v/v)	93.89 GHz	5 hours	30 mW	1.15 K	3.35 T	D$_2$O (5 mL)	N/A	17
Y-DOTP (176 mM) and Y-DO3A-NTs (143 mM)	OX063 (15 mM)	H$_2$O/glycerol(160 μL, 75/25, v/v)	94.125 GHz	N/A	100 mW	1.4 K	3.35 T	H$_2$O (4 mL)	3000	54
Y-DOTA (400 mM)	TEMPO (50 mM)	50/50 D$_2$O/glycerol-d_8	N/A	3 hours	N/A	1.05 K	5 T	N/A	3250	55
Various Y complexes ($\sim$200 mM)	OX063 (15 mM)	H$_2$O/glycerol (160 μL, 75/25, v/v)	N/A	3 hours	N/A	1.4 K	N/A	N/A	N/A	13
Various Y complexes (700–1500 mM)	Trityl radical (16.6 mM)	H$_2$O/glycerol (20–40 μL, 50/50, v/v)	94.118 GHz	75 min–2.5 hours	100 mW	1.4 K	N/A	EDTA in H$_2$O (4 mL, 850 μM)	246–1527	53
Y-DOTA (140–280 mM)	OX063 (15 mM)	H$_2$O/glycerol (40 μL, 50/50, v/v)	$\sim$94 GHz	Up to 10 hours	100 mW	1.4 K	3.35 T	H$_2$O (4 mL)	65,000	51
Y-^{13}CDOTA (325 mM)	OX063 (15 mM)	H$_2$O/glycerol (40 μL, 50/50, v/v)	94.16 GHz	5–7 hours	100 mW	1.4 K	3.35 T	H$_2$O (4 mL)	387–8040	52

This journal is © The Royal Society of Chemistry 2020

Chem. Soc. Rev., 2020, **49**, 6169–6185 | **6181**

able to monitor ^{13}C signal intensity as a function of microwave frequency and subsequent signal growth over increasing irradiation time, such systems are unable to monitor changes in ^{89}Y signals in a similar way. Therefore, finding the optimum microwave frequency and irradiation time required for optimum polarisation of ^{89}Y nuclei is challenging and involves the rapid melting and ejection of many separate samples for the buildup and NMR detection of ^{89}Y signal intensity. These technical challenges are reflected in the range of different ^{89}Y polarisation conditions reported in the literature to date (Table 5).[13,51–53]

Optimisation of these polarisation conditions can include modification of several factors including the organic radical used for polarisation transfer, the glassing matrix, concentrations, and irradiation time and frequency. Lumata et al. have performed a detailed study of the effect of these factors on ^{89}Y signal gains.[51] It was reported that using organic radicals with narrow electron paramagnetic resonance linewidths (such as trityl rather than nitroxyl radicals) yields more efficient polarisation transfer from the unpaired electron to the ^{89}Y target of interest.[51] Moreover, addition of an electron relaxing agent such as a Gd^{3+} salt can yield higher ^{89}Y polarisation by up to a factor of five (Fig. 9a).[51] This effect has been reported for other heteronuclei such as ^{13}C. Performing these optimisation steps is time consuming and challenging as ^{89}Y signal growth

cannot be monitored in situ, as previously discussed. For example, optimisation of polarising frequency and irradiation time involved d-DNP of 12 and 7 separate ^{89}Y-DOTA samples respectively.[51] Despite these challenges, by combination of various optimisation steps, including using optimum microwave frequencies, irradiation times, radical, Gd^{3+} additive and viscous glass forming solvents, ^{89}Y signals enhanced by a factor of 65 000 were achieved.[51]

Interestingly, the co-polarisation of sodium pyruvate-1-^{13}C or polarisation of ^{13}C-enriched ^{89}Y-DOTA has been used to provide information on the mechanism of signal enhancement. In these systems the growth of ^{13}C polarisation can be monitored in situ and this is correlated to the ^{89}Y signal gain (Fig. 9b).[51,52] The co-polarisation of ^{89}Y and ^{13}C nuclei may provide a way to indirectly monitor the growth of ^{89}Y polarisation and reliably predict the ^{89}Y signal gain upon rapid melting and ejection of the sample.

The hyperpolarisation of a wide range of yttrium containing complexes has been reported using d-DNP (Fig. 9c and Table 5).[11,53] These examples show that ^{89}Y chemical shift is highly dependent on its coordination environment with large ($\sim$80 ppm) shift differences reported for hyperpolarised ^{89}Y nuclei coordinated to various different macrocyclic ligands. Such high sensitivity of ^{89}Y chemical shift to molecular environment has been exploited to design hyperpolarised ^{89}Y pH
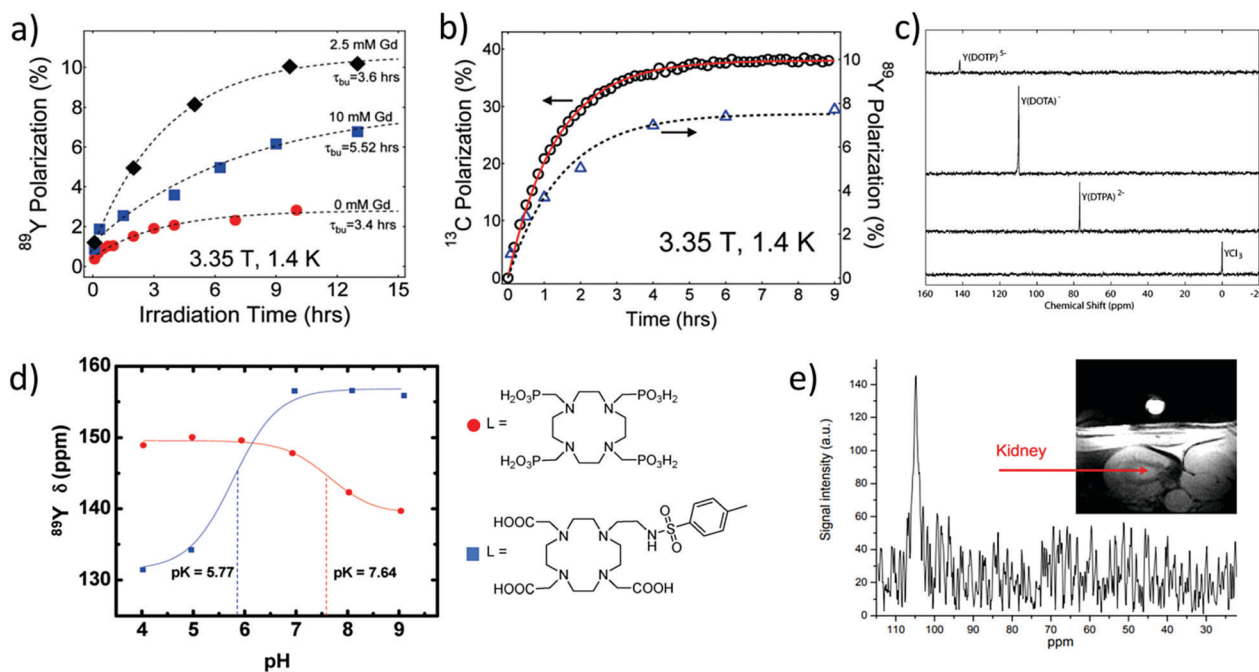

Fig. 9 Applications of hyperpolarised ^{89}Y complexes in MR. (a) Example polarisation buildup curves of 0.28 M Y-DOTA samples in a 1 : 1 glycerol/water glassing matrix doped with 15 mM trityl radical and Gd^{3+} (0, 2.5, and 10 mM). (b) Polarisation buildup of samples with 1-^{13}C pyruvate (left axis) and ^{89}Y-DOTA (right axis) doped with 15 mM trityl OX063 and 2.5 mM Gd^{3+} at 1.4 K and 3.35 T. Note that each data point in the ^{89}Y buildup curves in (a) and (b) represents a separate DNP experiment. (c) ^{89}Y NMR spectra collected at 29.4 MHz using a 14.1 T magnet of hyperpolarised yttrium complexes recorded with a 10° excitation pulse ~30 s after transfer from the DNP polariser to a 8 mm NMR tube. (d) ^{89}Y chemical shift dispersion of hyperpolarised Y-DOTP and YDO3A-NTs as a function of pH (9.4 T and 25 °C) and the corresponding structures of their ligands. (e) Y-DOTA hyperpolarised using DNP has been injected and imaged in a rat kidney. Reproduced with permission from (a) and (b) ref. 51. Copyright © 2011 American Chemical Society (c) ref. 53. Copyright © 2007 American Chemical Society (d) ref. 54. Copyright © 2010 American Chemical Society and (e) ref. 55. Copyright © 2010 International Society for Magnetic Resonance in Medicine.

6182 | Chem. Soc. Rev., 2020, 49, 6169–6185

This journal is © The Royal Society of Chemistry 2020

sensitive probes. Examples contain phosphonate and carboxylate groups, whose protonation state changes with pH, thereby affecting the molecular environment around the coordinated ^{89}Y ion and its subsequent chemical shift (Fig. 9d).[54] Other studies have utilised the differences in hyperpolarised ^{89}Y chemical shift that exist between free and complexed ions to measure complexation rates to the macrocyclic DOTAM ligand and the associated binding kinetics.[17]

It was not until 2016 that a quantitative link between ^{89}Y chemical shift and environment was outlined through studies on 23 complexes containing polyaminocarboxylate ligands. In this seminal work, an empirical equation was derived to accurately relate ^{89}Y chemical shift to the number and type of coordinating atoms.[13] Good agreement was found between ^{89}Y shifts predicted from this empirical equation and those observed for both thermal and hyperpolarised samples. Hyperpolarised ^{89}Y studies can therefore provide important information on complex kinetics and protonation states. It should also be noted that typical concentrations of ^{89}Y complexes detected in vitro in single scan hyperpolarised NMR spectra lie in the range 100 μM–7 mM, which are significantly higher than those which feature as PET tracers (see above). We are not aware of any detection limit for ^{89}Y HP-MRI, but note that this can be improved by future development of experimental set up, RF coil detection, and increased ^{89}Y signal gains.

Research into the hyperpolarisation of ^{89}Y is currently at the level of preliminary in vivo imaging studies. In an initial report, Y-DOTA was administered in a rat kidney to provide the first ^{89}Y MR images (Fig. 9e);[55] further examples in this direction are still pending. However, ^{89}Y chemical shift has proven to be highly sensitive to the molecular environment and it is expected that future uses of ^{89}Y as a probe for such changes in molecular environment can be envisaged. It has already been shown that ^{89}Y chemical shift of Y-EDTA can change by as much as ∼10 ppm in the presence of sodium lactate at pH 6.4 and 25 °C at 9.4 T.[13] Therefore, ^{89}Y complexes may serve a unique role as an in vivo probe for such biomolecules. Currently, DNP is a time consuming and expensive technique available only to a few research institutions. While no reports of ^{89}Y hyperpolarised with techniques other than DNP have been reported, advances in other hyperpolarisation techniques including the cheaper para-hydrogen based methods[50] may reflect exciting opportunities to target the hyperpolarisation of ^{89}Y.

Conclusions

The role of yttrium in medical applications, especially radiotherapy and medical imaging, has been frequently neglected. Yttrium can form a large number of complexes owing to its specific coordination and radiochemical properties which show a wide variety of features. To this end, yttrium complexes can provide a route to multimodal imaging in which the same ligands can be coordinated to ^{86}Y and used for PET, ^{90}Y and used for radiotherapy, and ^{89}Y and used for HP-MRI, with ^{89}Y chemical shifts extremely sensitive to molecular environment.

The former two methods have already found a number of applications in modern medical diagnostic and therapeutic procedures, which are briefly overviewed in this work. Nonetheless, owing to its versatile properties, yttrium's mostly abundant isotope ^{89}Y possesses properties suitable for NMR and MRI applications. Combined with hyperpolarisation, an emerging technique in modern NMR, yttrium offers a whole new avenue for molecular imaging studies based on metal chelates. All these methods together highlight the substantial contribution that yttrium has had, and will have, to biomedical research and clinical routines towards improving human health. With the most recent advances, the palette of its applications is expanding and further exciting progress is expected in the years to come.

Abbreviations

1B4M-DTPA	2-(p-SCN-benzoyl)-6-methyl-DTPA
CHX-A''-DTPA	trans-(S,S)-Cyclohexane-1,2-diamine-N,N-N',N',N''N''-pentaaceticacid
CN	Coordination number
CT	Computed tomography
DEPA	7-2-(Bis-carboxymethylamino)-ethyl-4,10-biscarboxymethyl-1,4,7,10-tetraazacyclododec-1-yl-acetic acid
DNP	Dynamic nuclear polarization
DTPA	Diethylenetriaminepentaacetic acid
DO3A	1,4,7,10-Tetraazacyclododecane-1,4,7-tricarboxylic acid
DO3A-NT	1-2'-(4-methylphenylsulfonylamino)ethyl-4,7,10-tris(carboxymethyl)-1,4,7,10-tetraazacyclododecane
DO3A-NTs	A DO3A derived ligand whose structure is shown in Fig. 9d (lower)
DOTA	1,4,7,10-Tetraazacyclododecane-1,4,7,10-tetracetic acid
DOTALAN	DOTA-lanreotide
DOTAM	1,4,7,19-Tetrakis(caramoylmethyl)-1,4,7,10-tetraazacyclododecane
DOTANOC	DOTA-1-NaI^3-octreotide
DOTATATE	DOTA-Tyr^3-octreotide
DOTATOC	DOTA-Phe^1-Tyr^3-octreotide
DOTP	1,4,7,10-Tetraazacyclododecane-1,4,7,10-tetra(methylene phosphonic acid)
EDTA	Ethylenediaminetetraacetic acid
EDTMP	Ethylenediamine tetra(methylene phosphonic acid)
EGFR	Epidermal growth factor receptors
^{18}FDG	Fluorodeoxyglucose (^{18}F)
HER2	A human epidermal growth factor receptors
HILIC-ICP-MS	Hydrophilic interaction chromatography and inductively coupled plasma mass spectrometry
HP-MRI	Hyperpolarised magnetic resonance imaging
LNCaP	Androgen sensitive human prostate adeno-carcinoma cell line

This journal is © The Royal Society of Chemistry 2020

Chem. Soc. Rev., 2020, 49, 6169–6185 | 6183

MP2346	A Gastrin-releasing peptide receptors targeted peptide
MR	Magnetic resonance
NETA	2-{4,7-Biscarboxymethyl(1,4,7)triazacyclonona-1-yl-ethyl}carbonylmethylaminoacetic acid
NMR	nuclear magnetic resonance
OCTAPA	N,N'-bis(6-carboxy-2-pyridylmethyl)-ethylenediamine-N,N'-diacetic acid
OX063	Tris8-carboxyl-2,2,6,6-benzo(1,2-d:4,5-d)-bis(1,3)dithiole-4-ylmethyl sodium salt
PCTA	3,6,9,15-Tetraazabicyclo9.3.1pentadeca-1-(15),11,13-triene-3,6,9-triacetic acid
PET	Positron emission tomography
PRRT	Peptide receptor radionuclide therapy
ReCCMSH	A cyclic analogue of α-melanocyte stimulating hormone
RF	Radiofrequency
SAP	Monocapped square antiprism
SEM	Scanning electron microscope
SPECT	Single-photon emission CT
TEMPO	(2,2,6,6-Tetramethylpiperidin-1-yl)oxyl or (2,2,6,6-tetramethylpiperidin-1-yl)oxidanyl
TSAP	Monocapped twisted square antiprism
TTP	Tricapped trigonal prism
VEGF-A	Vascular endothelial growth factor A
YAG	Yttrium aluminium garnet

Conflicts of interest

There are no conflicts to declare.

Acknowledgements

Notes and references

1 H. Schumann, A. Heim, J. Demtschuk and S. H. Mühle, *Organometallics*, 2003, **22**, 118–128.
2 S. Cotton, *Lanthanide and actinide chemistry*, John Wiley & Sons Ltd., Chichester, 2006.
3 N. B. Mikheev, L. Auerman, I. A. Rumer, A. N. Kamenskaya and M. Z. Kazakevich, *Russ. Chem. Rev.*, 1992, **61**, 990.
4 F. G. N. Cloke, *Chem. Soc. Rev.*, 1993, **22**, 17–24.
5 C. L. Wright, J. Zhang, M. F. Tweedle, M. V. Knopp and N. C. Hall, *BioMed Res. Int.*, 2015, **2015**, 1–11.
6 T. H. Bokhari, M. B. Butt, S. Hina, M. Iqbal, M. Daud and M. Imran, *J. Radioanal. Nucl. Chem.*, 2017, **314**, 1487–1496.
7 S. Hirano, N. Kodama, K. Shibata and K. T. Suzuki, *Toxicol. Appl. Pharmacol.*, 1993, **121**, 224–232.
8 A. S. Merbach, L. Helm and E. Toth, *The Chemistry of Contrast Agents in Medical Magnetic Resonance Imaging*, John Wiley & Sons Ltd., 2013.
9 K. Kumar, C. A. Chang, L. Francesconi, D. Dischino, M. Malley, J. Gougoutas and M. F. Tweedle, *Inorg. Chem.*, 1994, **33**, 3567–3575.
10 M. Le Fur, N. J. Rotile, C. Correcher, V. Clavijo Jordan, A. W. Ross, C. Catana and P. Caravan, *Angew. Chem., Int. Ed.*, 2019, **59**, 1474–1478.
11 Z. Baranyai, G. Tircsó and F. Rösch, *Eur. J. Inorg. Chem.*, 2020, 36–56.
12 T. I. Kostelnik and C. Orvig, *Chem. Rev.*, 2019, **119**, 902–956.
13 Y. Xing, A. K. Jindal, M. Regueiro-Figueroa, M. Le Fur, N. Kervarec, P. Zhao, Z. Kovacs, L. Valencia, P. Pérez-Lourido, R. Tripier, D. Esteban-Gómez, C. Platas-Iglesias and A. D. Sherry, *Chem. – Eur. J.*, 2016, **22**, 16657–16667.
14 D. Parker, K. Pulukkody, F. C. Smith, A. Batsanov and J. A. K. Howard, *Dalton Trans.*, 1994, 689–693.
15 C. F. G. C. Geraldes, A. M. Urbano, C. Carmen Alpoim, M. A. Hoefnagel and J. A. Peters, *J. Chem. Soc., Chem. Commun.*, 1991, 656–658.
16 E. W. Price and C. Orvig, *Chem. Soc. Rev.*, 2014, **43**, 260–290.
17 P. Miéville, S. Jannin, L. Helm and G. Bodenhausen, *J. Am. Chem. Soc.*, 2010, **132**, 5006–5007.
18 A. Nystrom and M. Thoennessen, *At. Data Nucl. Data Tables*, 2012, **98**, 95–119.
19 J. Wike, C. Guyer, D. Ramey and B. Phillips, *Int. J. Radiat. Appl. Instrum., Part A*, 1990, **41**, 861–865.
20 K. Kettern, K.-H. Linse, S. Spellerberg, H. H. Coenen and S. M. Qaim, *Radiochim. Acta*, 2002, **90**, 845–849.
21 J. Lellouche, A. Friedman, A. Gedanken and E. Banin, *Int. J. Nanomed.*, 2012, **7**, 5611–5624.
22 A.-E. Borgonovo, A. Fabbri, V. Vavassori, R. Censi and C. Maiorana, *Med. Oral Patol. Oral Cir. Bucal*, 2012, **17**, e981–e987.
23 E. Schena, P. Saccomandi and Y. Fong, *J. Funct. Biomater.*, 2017, **8**, 19.
24 P. Hilgard, M. Hamami, A. E. Fouly, A. Scherag, S. Müller, J. Ertle, T. Heusner, V. R. Cicinnati, A. Paul and A. Bockisch, *Hepatology*, 2010, **52**, 1741–1749.
25 Z. Nosrati, A. R. Khanchi and S. Sheybani, *J. Radioanal. Nucl. Chem.*, 2014, **301**, 373–382.
26 A. S. Mahmoud-Ahmed and J. H. Suh, *Pituitary*, 2002, **5**, 175–180.
27 J. Rosenstock, R. Jung, F. Doyle, K. Mashiter and G. Joplin, *J. R. Soc. Med.*, 1982, **75**, 209–210.
28 W. Taylor, M. Corkill and C. Rajapaske, *Br. J. Rheumatol.*, 1997, **36**, 1100–1105.
29 M. Heim, E. Goshen, Y. Amit and U. Martinowitz, *Haemophilia*, 2001, **7**, 36–39.
30 L. Nisa, G. Savelli and R. Giubbini, *Ann. Nucl. Med.*, 2011, **25**, 75–85.
31 J. Kunikowska, L. Królicki, A. Hubalewska-Dydejczyk, R. Mikołajczak, A. Sowa-Staszczak and D. Pawlak, *Eur. J. Nucl. Med. Mol. Imaging*, 2011, **38**, 1788–1797.

6184 | *Chem. Soc. Rev.*, 2020, **49**, 6169–6185

This journal is © The Royal Society of Chemistry 2020

32 P. M. Smith-Jones, C. Bischof, M. Leimer, D. Gludovacz, P. Angelberger, T. Pangerl, M. Peck-Radosavljevic, G. Hamilton, K. Kaserer and A. Kofler, *Endocrinology*, 1999, **140**, 5136–5148.

33 D. Wild, J. S. Schmitt, M. Ginj, H. R. Mäcke, B. F. Bernard, E. Krenning, M. De Jong, S. Wenger and J.-C. Reubi, *Eur. J. Nucl. Med. Mol. Imaging*, 2003, **30**, 1338–1347.

34 L. Villard, A. Romer, N. Marincek, P. Brunner, M. T. Koller, C. Schindler, Q. K. Ng, H. R. Mäcke, J. Müller-Brand and C. Rochlitz, *J. Clin. Oncol.*, 2012, **30**, 1100–1106.

35 F. Rösch, H. Herzog and S. M. Qaim, *Pharmaceuticals*, 2017, **10**, 56.

36 F. Morschhauser, J. Radford, A. Van Hoof, B. Botto, A. Z. S. Rohatiner, G. Salles, P. Soubeyran, H. Tilly, A. Bischof-Delaloye and W. L. J. van Putten, *J. Clin. Oncol.*, 2013, **31**, 1977–1983.

37 M. Saki, M. Toulany, W. Sihver, M. Zenker, J. M. Heldt, B. Mosch, H. J. Pietzsch, M. Baumann, J. Steinbach and H. P. Rodemann, *Strahlenther. Onkol.*, 2012, **188**, 823–832.

38 Z. Liu, Y. Liu, B. Jia, H. Zhao, X. Jin, F. Li, X. Chen and F. Wang, *Mol. Cancer Ther.*, 2010, **9**, 1535–7163.

39 E. W. Price, K. J. Edwards, K. E. Carnazza, S. D. Carlin, B. M. Zeglis, M. J. Adam, C. Orvig and J. S. Lewis, *Nucl. Med. Biol.*, 2016, **43**, 566–576.

40 S. C. Golstein, K. Muylle, M. Vercruyssen, C. Spilleboudt, A. de Wind and D. Bron, *Eur. J. Haematol.*, 2018, **101**, 415–417.

41 S. S. Gambhir, J. Czernin, J. Schwimmer, D. H. Silverman, R. E. Coleman and M. E. Phelps, *J. Nucl. Med.*, 2001, **42**, 1S–93S.

42 A. A. Attarwala, F. Molina-Duran, K.-A. Büsing, S. O. Schönberg, D. L. Bailey, K. Willowson and G. Glatting, *PLoS One*, 2014, **9**, e110401.

43 A. S. Pasciak, A. C. Bourgeois, J. M. McKinney, T. T. Chang, D. R. Osborne, S. N. Acuff and Y. C. Bradley, *Front. Oncol.*, 2014, **4**, 38.

44 T. K. Nayak and M. W. Brechbiel, *Med. Chem.*, 2011, **7**, 380–388.

45 H. G. Buchholz, H. Herzog, G. J. Förster, H. Reber, O. Nickel, F. Rösch and P. Bartenstein, *Eur. J. Nucl. Med. Mol. Imaging*, 2003, **30**, 716–720.

46 D. W. Schneider, T. Heitner, B. Alicke, D. R. Light, K. McLean, N. Satozawa, G. Parry, J. Yoo, J. S. Lewis and R. Parry, *J. Nucl. Med.*, 2009, **50**, 435–443.

47 T. K. Nayak, K. Garmestani, K. E. Baidoo, D. E. Milenic and M. W. Brechbiel, *Int. J. Cancer*, 2011, **128**, 920–926.

48 F. Rösch, H. Herzog, C. Plag, B. Neumaier, U. Braun, H.-W. Müller-Gärtnere and G. Stöcklin, *Eur. J. Nucl. Med.*, 1996, **23**, 958–966.

49 G. Sgouros, *Med. Phys.*, 1998, **25**, 1487–1490.

50 P. Nikolaou, B. M. Goodson and E. Y. Chekmenev, *Chem. – Eur. J.*, 2015, **21**, 3156–3166.

51 L. Lumata, A. K. Jindal, M. E. Merritt, C. R. Malloy, A. D. Sherry and Z. Kovacs, *J. Am. Chem. Soc.*, 2011, **133**, 8673–8680.

52 L. Lumata, M. Merritt, C. Malloy, A. D. Sherry and Z. Kovacs, *Appl. Magn. Reson.*, 2012, **43**, 69–79.

53 M. E. Merritt, C. Harrison, Z. Kovacs, P. Kshirsagar, C. R. Malloy and A. D. Sherry, *J. Am. Chem. Soc.*, 2007, **129**, 12942–12943.

54 A. K. Jindal, M. E. Merritt, E. H. Suh, C. R. Malloy, A. D. Sherry and Z. Kovács, *J. Am. Chem. Soc.*, 2010, **132**, 1784–1785.

55 M. E. Merritt, M. Mishkovsky, T. Cheng, A. Jindal, Z. Kovacs, C. Malloy, R. Gruetter, A. D. Sherry and A. Comment, *Proc. Intl. Soc. Mag. Reson. Med.*, 2010, **18**, 1030.

This journal is © The Royal Society of Chemistry 2020

Chem. Soc. Rev., 2020, **49**, 6169–6185 | 6185